Comparison of Converging and Diverging Radial Flow for Measuring Cell Adhesion

Aaron S. Goldstein and Paul A. DiMilla
Dept. of Chemical Engineering, Colloids, Polymers and Surfaces Program, and Center for Light Microscope Imaging and Biotechnology, Carnegie Mellon University, Pittsburgh, PA 15213

Radial flow between parallel surfaces produces a spatially dependent wall shear stress that permits investigation of cell adhesion for a range of shear simultaneously. The maximum for this range is limited by accurate prediction of fluid mechanics at small radial positions. Numerical and analytical models for predicting fluid mechanics demonstrate that corner and inertial effects at small radial positions are not only significant but differ with the direction of flow (i.e., converging vs. diverging). For diverging flow from an axially oriented inlet, the recirculation zone downstream of the corner disturbs streamlines at small radial positions. With converging flow this recirculation zone is confined to the axially oriented outlet. Also, inertia contributes positively for converging flow, enhancing the magnitude of shear stress, but negatively for diverging flow. Experiments with cells support the validity of this analysis: the strength of cell adhesion does not vary with direction or magnitude of flow.

Introduction

A fundamental understanding of the key issues that regulate the strength of cell–cell and cell–substratum interactions is invaluable to the fields of medicine and bioengineering. For example, in the circulatory system the flowing blood maintains a hydrodynamic shear stress on the lumen of blood vessels. Consequently, processes here, such as the immune response (Finger et al., 1996), formations of blood clots (McIntire et al., 1991), and adhesion of infectious bacteria to tissues (Dickinson and Cooper, 1995), require strong adhesive interactions. In addition, the rationale for engineered materials, such as polymeric supports for artificial blood vessels (Williams et al., 1994) and therapies to suppress immune responses (Sadahiro et al., 1993), has been to regulate adhesive interactions.

Numerous approaches have been developed to examine cell–cell and cell–substratum adhesion quantitatively that involve applying a detaching force but differ in how the force is generated and the direction in which it is applied. Micropipette aspiration (MPA) (Evans et al., 1991) and centrifugation (Chu et al., 1994) have been used to apply forces normal and parallel to the plane of contact. However the former technique restricts measurements to individual cells, and the latter approach does not allow observation of the process of detachment. One technique that permits observation *in situ* of many cells simultaneously is detachment under hydrodynamic shear in a flow chamber. Hydrodynamic shear imparts both a drag force and a torque on adherent cells (Hammer and Lauffenburger, 1987), which make quantitative comparison to studies by MPA and centrifugation difficult. However, this technique is directly applicable to the study of phenomena in the cardiovascular system.

Among the various types of flow chambers, the radial-flow chamber (RFC) (Moller, 1963; Fowler and McKay, 1980; Cozens-Roberts et al., 1990; Dickinson and Cooper, 1995; Rezania et al., 1997; Goldstein and DiMilla, 1997) is one of a few designs that generates a spatially dependent range of shear stresses. (Alternative geometries with this capacity have been suggested by Usami et al. (1992) and Xiao and Truskey (1996).) The key difference between the RFC and a conventional parallel-plate flow chamber (e.g., McIntire et al., 1991; van Kooten et al., 1992) is that whereas the latter uses laminar flow through a conduit of constant cross section to produce a uniform shear stress, the former utilizes axisymmetric radial flow through a cross-section that varies proportionally with radial position to produce a shear stress that decreases with increasing radial position (Figure 1). The advantage with

Correspondence concerning this article should be addressed to P. A. DiMilla.

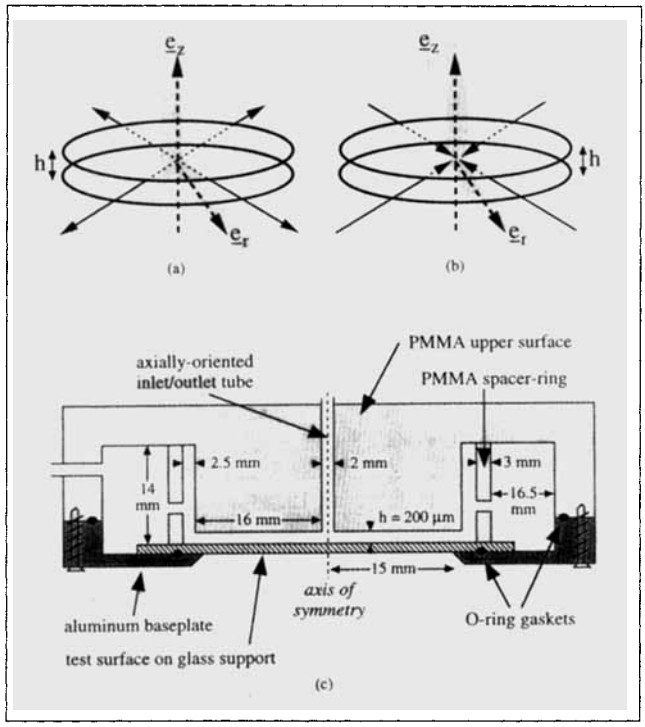

Figure 1. Radial-flow geometry.

(a) Two parallel surfaces in the $r-\theta$ plane separated by a gap, h. Dashed arrows represent axial, e_z, and radial, e_r, components of this two-dimensional cylindrical geometry. Solid arrows illustrate diverging radial flow. (b) Same as (a) except solid arrows illustrate converging radial flow. (c) The experimental flow chamber for radial flow between parallel surfaces. A cylindrical spacer ring (with holes to permit flow) is fused to upper surface and maintains uniform gap. A narrow hole in the upper surface serves as an inlet for diverging flow and an outlet for converging flow and defines the axis of symmetry. A large hole in the base plate permits observation *in situ* with an inverted microscope. Dimensions listed here serve as basis for both the numerical and experimental studies presented.

the RFC is that adhesion can be examined over a broad range of shear stresses simultaneously.

For quantitative analysis of adhesion in an RFC, the shear stresses that can be examined are limited to the range that can be predicted confidently. For example, the analytical solution for creeping flow (Fowler and McKay, 1980; Kuo and Lauffenburger, 1993; Dickinson and Cooper, 1995) is reliable for low Reynolds numbers but restricts the maximum shear stress that can be reported. In order to report larger shear stresses reliably, inertial (Fryer et al., 1985) and end effects should be considered. In our previous work we investigated the significance of these effects for diverging flow (i.e., flow entering through an axially oriented inlet and spreading radially outward) by considering two additional models; an analytical solution for creeping flow with a first-order inertial correction (Jackson and Symmons, 1965; Rezania et al., 1997), and a discretized numerical model using Fluent (Goldstein and DiMilla, 1997). Through a comparison of these models we identified three distinct regions within the chamber: at large radial positions the assumption of creeping flow is valid, at intermediate position inertial effects are significant and act to reduce wall shear stresses, and at small radial positions flow profiles are dominated by inlet effects (and shear stresses could not be accurately predicted).

In this study we apply the two analytical models—creeping flow and inertially corrected creeping flow—and the numerical simulation package, Fluent, to examine the effect of reversing the direction of flow: operating the RFC with converging rather than diverging radial flow (Figure 1). We show that the range of shear stresses that can be estimated accurately with converging flow is more than twice that with diverging flow. We find that at large radial positions—where creeping flow is valid—shear stress is independent of direction of flow. At intermediate positions where inertia is important it increases the magnitude of shear stresses for converging flow but decreases it for diverging flow. Finally, at small radial positions outlet effects with converging flow are profoundly different from inlet effects with diverging flow. In addition, we present experimental detachment studies that confirm that the measured strength of adhesion of individual cells to a model biomaterial is independent of both direction of flow and volumetric flow rate.

Mathematical Modeling

To evaluate the difference between diverging and converging flow we compared the analytical solutions for creeping flow and creeping flow with an inertial correction with numerical predictions using Fluent, a finite difference package. In our previous study we compared these models for diverging flow using the dimensions of our experimental RFC and three volumetric flow rates (Goldstein and DiMilla, 1997); in this study we examine converging flow and compare it to diverging flow. Our primary objective is to identify the maximum shear stress that can be predicted both accurately and analytically, and we select a 5% departure of the inertially corrected solution for creeping flow from the numerical prediction as our criterion. (We note that approaches exist to verify numerical solutions that can potentially increase the maximum shear stresses that can be accurately predicted, but they are computationally expensive and not important to most of the results in this study).

Analytical models of flow in an RFC

In cylindrical coordinates, radial flow is constrained between two parallel walls in the $r-\theta$ plane at $z = \pm h/2$. The creeping-flow solution to the Navier–Stokes equation for an incompressible Newtonian fluid is purely radial with a fluid velocity that is parabolic with respect to the z-axis and varies inversely with radial position, r,

$$v(r,z) = \frac{3Q}{4\pi hr}\left(1-\frac{4z^2}{h^2}\right)e_r. \tag{1}$$

Here we have incorporated volumetric flow rate, $Q = 2\pi r\int_{-h/2}^{h/2} v(r,z)\,dz\cdot e_r$, into the expression because it is independent of position. Note that Q is positive for diverging flow and negative for converging flow. Thus, Eq. 1 predicts that streamlines that emanate radially from a segment of the axis of symmetry, $r = 0$ and $-h/2 < z < h/2$ for diverging flow (Figure 1a), converge on this same segment of the axis of

symmetry for converging flow (Figure 1b). By defining the wall shear stress, τ_w, as the product of viscosity, μ, and the component of the rate of strain tensor for stress in the positive radial direction acting on the surface $z = \pm h/2$ pointing into the fluid phase, the solution for creeping flow is

$$\tau_w = \frac{3\mu Q}{\pi h_r^2}. \tag{2}$$

By this definition τ_w for converging flow ($Q < 0$) and diverging flow ($Q > 0$) are equal in magnitude, but the former is always negative and the latter always positive.

Wall shear stress also can be described dimensionlessly. Because the characteristic spatial dimension for our system is the gap height, h, we define a dimensionless position $R = r/h$, and a reference wall shear stress,

$$\tau_w^* = \tau_{w(r=h)} = \frac{3\mu Q}{\pi h^3}. \tag{3}$$

Normalizing Eq. 2 by the reference wall shear stress leads to the expression

$$T_w = \frac{\pi_w}{\tau_w^*} = \frac{1}{R}. \tag{4}$$

Note that this dimensionless shear stress for creeping flow is a geometric relationship independent of fluid properties.

Although the solution for creeping flow has been used to interpret data for cell detachment (e.g., Kuo and Lauffenburger 1993; Dickinson and Cooper, 1995), one criticism has been that this solution neglects inertial effects at small radial positions where the radial gradient in velocity is large (Fryer et al., 1985). Several approaches to account for inertial effects can be found in the literature. Two among them, a power-series expansion in radial position for two-dimensional flow (Hunt and Torbe, 1962; Jackson and Symmons, 1965) and a first-order inertial correction to the one-dimensional solution (accomplished by substituting the solution for creeping flow into the inertial terms of the Navier–Stokes equation) (Jackson and Symmons, 1966; Rezania et al., 1997), yield the same first-order correction for radial component for velocity, v_r,

$$v_r(r,z) = \frac{3Q}{4\pi rh}\left(1-\frac{4z^2}{h^2}\right) - \frac{9\rho Q^2}{64\pi^2 r^3}\left(\frac{64z^6}{30h^6} - \frac{16z^4}{6h^4} + \frac{44z^2}{70h^2} - \frac{1}{42}\right). \tag{5}$$

For this solution the corresponding wall shear stress (in the positive radial direction acting on the surface $z = \pm h/2$ pointing into the fluid) is

$$\tau_w = \frac{3\mu Q}{\pi h^2 r} - \frac{3\rho Q^2}{70\pi^2 h r^3}. \tag{6}$$

Because the volumetric flow rate is positive for diverging radial flow and negative for converging flow, the predicted shear stresses for diverging and converging flow are different. With diverging flow the first and second terms have opposite signs, but with converging flow the signs are the same. Consequently, the magnitude of shear stress for converging flow is predicted always to exceed that for diverging flow at a given radial position and magnitude of volumetric flow rate. As with the solution for creeping flow, the inertially corrected solution for creeping flow can be normalized by the reference wall shear stress (Eq. 3), yielding

$$T_w = \frac{1}{R} - \frac{Re_h}{70R^2}. \tag{7}$$

The first term here is the same as in Eq. 4, but the second term, which represents inertial effects normalized by viscous shear, is proportional to Reynolds number. Here we have defined Re_h as the Reynolds number, $Re = \rho Q/\mu r$ (Cozens-Roberts et al., 1990; Dickinson and Cooper, 1995), for the reference condition $r = h$,

$$Re_h = Re_{(r=h)} = \frac{\rho Q}{\pi \mu h}. \tag{8}$$

We use Re_h because it describes only the fluid mechanical properties; in contrast Re depends on radial position, a parameter we wish to examine independently. (In our previous work we defined a Reynolds number with respect to the diameter of the inlet, $Re_d = Re_h/2.5$ (Goldstein and DiMilla, 1997).) Note also that Re and Re_h are proportional to Q, and therefore will be positive for diverging flow and negative for converging flow.

We can evaluate the relative significance of the inertial correction by comparing the first and second terms. If we set the constraint that the solution for creeping flow is reasonable when the magnitude of the second term is less than 5% of the first, rearrangement of Eq. 6 leads to the inequality

$$r > \left(\frac{2\rho |Q| h}{7\pi\mu}\right)^{0.5}. \tag{9a}$$

In dimensionless form, from Eq. 7, this inequality becomes

$$R > \left(\frac{2|Re_h|}{7}\right)^{0.5}. \tag{9b}$$

The physical meaning of these expressions is that inertial effects become significant at larger radial positions with increasing volumetric flow rate or gap height.

One limitation with the analytical solutions for creeping flow (Eq. 1) and creeping flow with a first-order correction (Eq. 5) is that these solutions have assumed that flow either originates from or terminates at a segment of the axis of symmetry, $r = 0$; $-h/2 < z < h/2$. In order to apply this geometry an axially oriented tube is required at the axis of symmetry to serve as either an inlet or outlet (depending upon the direction of flow) (Figure 1c). Therefore, at small radial positions we would expect the fluid mechanics to be dominated

by the transition between axial and radial flow. To consider such influences requires numerical modeling to estimate the effects of flow around corners.

Numerical modeling of flow in an RFC

Laminar flow was simulated using the numerical modeling package, Fluent (Lebanon, NH). For diverging radial-flow a gap height of 0.2 mm and radius of 16 mm and an inlet tube 3 mm in length and 1 mm in radius was modeled using a Cartesian grid of 151×78 nodes. Grid spacing was refined geometrically near walls to improve accuracy where gradients were large. For converging radial-flow an axially oriented outlet tube with length of 1 mm was sufficient to model end effects and, consequently, a smaller Cartesian grid (91×78 nodes) could be used. Viscosity and density were selected for a dilute aqueous solution, $\mu = 0.91$ cP and $\rho = 1.00$, respectively. Volumetric flow rates of 1.43, 2.15 and 2.86 mL/s (corresponding to reference Reynolds numbers, Re_h, of 2500, 3750, and 5000, respectively) were examined because they are typical for our experiments with cells. (Note that these volumetric flow rates also ensured laminar flow in the axially oriented tube: Reynolds numbers here were 1000, 1500, and 2000, respectively. Re_h is listed because it neither depends on the size of the axially oriented tube nor varies with radial position. The relevant parameter to describe radial flow is the local Reynolds number, Re, which has a value of $Re_h/5$ at the edge of our axially oriented tube and decreases with increasing radial position). The boundary condition at the inlet was a fully developed parabolic flow at the chosen volumetric flow rate. The criterion for convergence was a sum of dimensionless residuals of less than 5×10^{-5}.

A separate model was developed to evaluate inlet effects for converging flow caused by the corner of the upper surface at a radial position of 16 mm (Figure 1c). In cylindrical coordinates, the region that was modeled was 1.2 mm in axial length and extended radially from 10 mm to 18.5 mm. The region upstream of the corner was modeled as an axially oriented annulus 1 mm long between walls at radial positions of 16 and 18.5 mm. The portion of the radial-flow chamber downstream from the corner from radius of 16 mm to 10 mm was modeled to determine the extent to which inlet effects propagated into the RFC. A Cartesian grid of 91×79 nodes and grid spacing was refined geometrically near walls. Fluid properties were the same as given earlier, the boundary condition at the inlet was a uniform flow profile, and only the maximum volumetric flow rate from the previous study (2.86 mL/s) was examined. For these calculations convergence was acceptable when the sum of dimensionless residuals was less than 4×10^{-4}.

Experimental Methods

Experimental studies were performed to verify that the measured strength of cell adhesion was independent of the magnitude and direction of flow. The preparation of cells and test surfaces—self-assembled monolayers (SAMs) of dodecanethiolate—and analysis of data were performed as described in detail previously (Goldstein and DiMilla, 1997) with two modifications: test surfaces were preincubated with fibronectin (an extracellular matrix protein known to promote adhesion), and cells were incubated with surfaces for 60 min before initiation of shear. SAMs of alkanethiolates were used because the physical and chemical properties are well defined and, consequently, are excellent model surfaces for examining interfacial phenomena such as protein adsorption and cell adhesion (DiMilla et al., 1994). Prior to assembly into the radial-flow chamber, freshly prepared SAMs were incubated with a solution of 5 μg/mL fibronectin in a phosphate-buffered saline solution (pH = 7.4) at room temperature (23°C) for 60 min. An O-ring gasket was placed on the surface to define a region 20 mm in radius and to contain the solution within a cylindrical volume of height 3 mm. Near the end of incubation the test surface was assembled carefully into the chamber to ensure that the incubated region did not pass through an air/water interface. After the RFC was assembled the surface was rinsed well with medium for detachment Hank's buffered salt solution with 1 mM CaCl, pH = 7.3). Next, Swiss 3T3 murine fibroblasts (CCL92) (American Type Cultures Collections, Rockville, MD, passage 125), were introduced gently into the RFC by syringe through the axially oriented tube at the axis of symmetry and allowed to incubate with the test surface for 60 min at room temperature prior to shear. Hydrodynamic shear was initiated rapidly by turning a three-way valve and maintained at a constant volumetric flow rate for 5 min.

Strength of adhesion was evaluated quantitatively by first comparing pairs of images collected prior to and after flow along the four primary axes at 0.5-mm intervals from radial positions of 3 mm to 15 mm. Data for the four axes were combined for each radial position to determine a number average fraction of cells that resisted detachment, FA, as a function of radial position. Next, the inertially corrected solution for creeping flow (Eq. 6) was used to calculate the wall shear stress corresponding to each radial position investigated. The resulting shear-dependent pattern of adhesion was sigmoidal (decreasing from unity to zero with increasing shear stress), a shape that Truskey and Pirone (1990) postulated reflects an underlying probability distribution of strengths of adhesion. Finally, for each experiment the best fit of the integral of a normal distribution,

$$FA(\tau_w) = \frac{1}{(2\pi\sigma_{\tau_w})^{0.5}} \int_{\tau=\tau_w}^{\tau\rightarrow} \exp\left[\frac{-(\tau-\tau_{wc})^2}{2\sigma_{\tau_w}^2}\right] d\tau, \quad (10)$$

was used to determine rigorously two parameters characterizing cell adhesion. We define the mean of the distribution function, τ_{wc}, as the mean strength of cell adhesion; it corresponds to the shear stress necessary to detach 50% of the cells. We refer to the standard deviation, σ_{τ_w}, as the heterogeneity in the strength of cell adhesion. We note that Eq. 10 is not the only model that has been proposed to describe shear-dependent patterns of adhesion (e.g., Truskey and Pirone, 1990; Rezania et al., 1997). We have compared the integrals of normal and log-normal distribution functions and found that they describe the data equally well; however, the latter approach consistently predicts a slightly lower mean strength of adhesion (Goldstein and DiMilla, 1997).

Results and Discussion

Comparison of streamlines for diverging and converging radial flow

Numerical calculations were performed to predict the fluid mechanics for laminar converging flow in the RFC for volumetric flow rates of 1.43, 2.15, and 2.86 mL/s. Streamlines predict qualitatively indistinguishable flow patterns for the three flow rates examined (Figure 2). At large radial positions the streamlines are parallel with the radial axis and consistent with the one-dimensional solution for creeping flow. However, at small radial positions the streamlines are dominated by the presence of the corner at 1 mm. In addition, the numerical model predicts the presence of two stable recirculation zones for laminar flow: one at the lower surface below the outlet (the region in Figure 2 devoid of streamlines at $r < 1$ mm) and one at the wall of the axially oriented tube just above the corner. Streamlines for diverging flow differ significantly with those for converging flow. For diverging flow the transition region from axial to radial flow (including a recirculation zone) is predicted to extend to larger radial positions with increasing volumetric flow rate (Figure 3). A comparison of Figures 2 and 3 reveals the fundamental advantage of converging radial-flow: with converging flow the range of radial positions affected by the axial-oriented tube is significantly smaller. Thus, we would expect the accuracy of the analytical solutions to extend to smaller radial positions and, correspondingly, larger wall shear stresses.

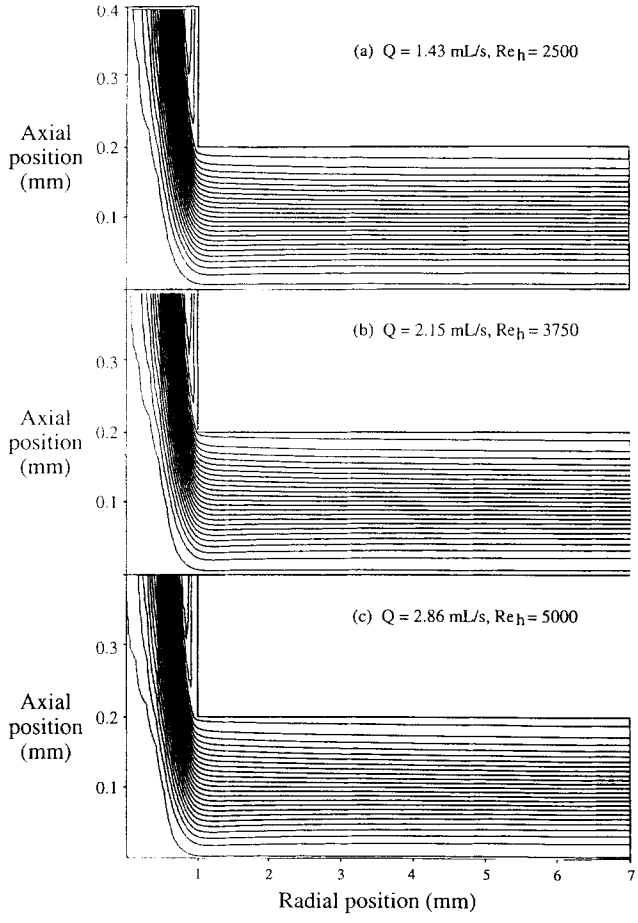

Figure 2. Streamlines for converging flow.

Predicted effect of reference Reynolds number, Re_h, for a dilute saline solution ($\rho = 1.00$ g/mL; $\mu = 0.91$ cP) in an RFC.

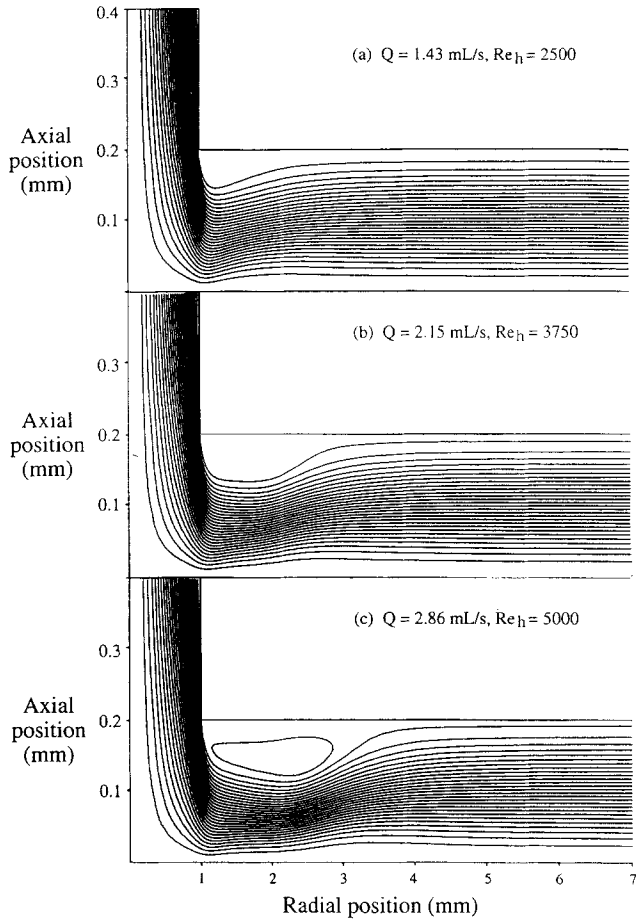

Figure 3. Streamlines for diverging flow.

Predicted effect of reference Reynolds number, Re_h, for a dilute saline solution ($\rho = 1.00$ g/mL; $\mu = 0.91$ cP) in an RFC.

Comparison of numerical and analytical models for wall shear stress for diverging and converging flow

The magnitude of the shear stress predicted numerically was compared to the analytical solutions for both creeping flow and creeping flow with an inertial correction for both diverging and converging flow for volumetric flow rates of 1.43, 2.15, and 2.86 mL/s (Figure 4). The magnitudes of wall shear stress for the three models also are shown in dimensionless form to demonstrate the effect of Reynolds number, Re_h (Figure 5). From Eq. 4 the model for creeping flow reduces to a hyperbola and is independent of the direction of flow. Curves for the inertially corrected analytical solution for converging flow demonstrate a positive deviation from creeping flow with increasing Re_h and decreasing dimensionless position, R (Figure 5a). The numerical model predicts a similar positive deviation but with a maximum corresponding to the edge of the inlet ($R = 5$). For diverging flow (Figure 5b) the inertially corrected solution for creeping flow demonstrates a negative deviation (equal in magnitude to the positive deviation with converging flow). The numerical model

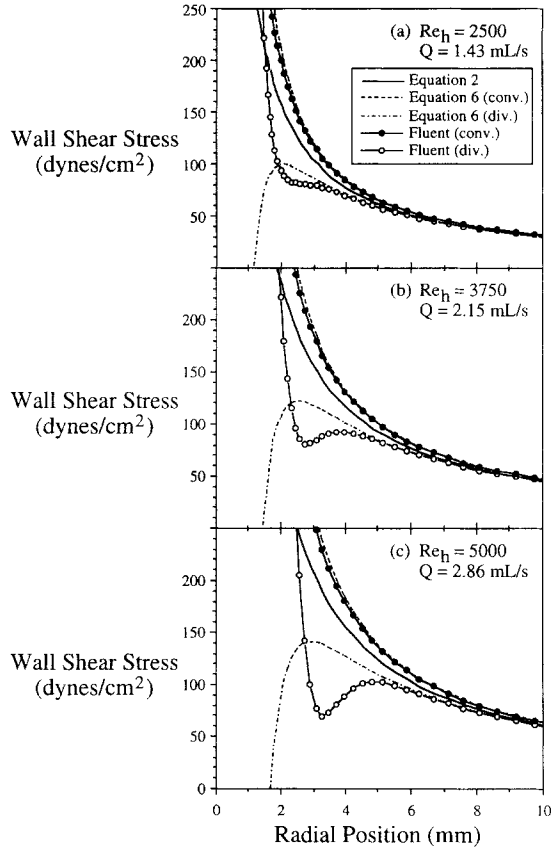

Figure 4. Wall shear stresses predicted for converging and diverging flow for various reference Reynolds numbers, Re_h.

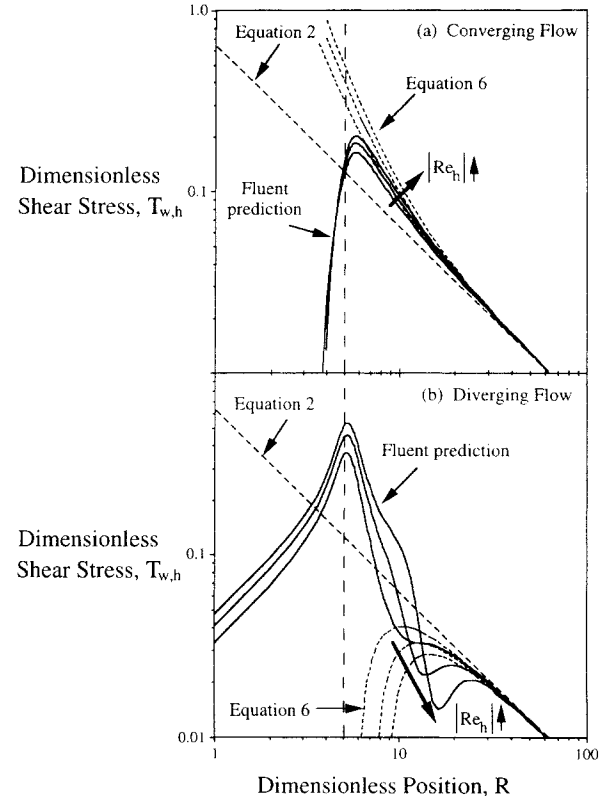

Figure 5. Effect of reference Reynolds number, Re_h, on predictions of shear stress.

(a) Converging radial flow. (b) Diverging radial flow. Predictions of dimensionless shear stresses are shown for Re_h = 2,500, 3,750, and 5,000 (Q = 1.43, 2.15, and 2.86 mL/s, respectively), with the arrow indicating the direction of increasing Reynolds number. The dashed vertical line at $R = 5$ corresponds to the corner between chamber and axially oriented tube.

confirms this negative deviation but also predicts a local minimum—associated with flow around the recirculation zone—that increases in radial position and decreases in magnitude with increasing Re_h.

These plots demonstrate two advantages associated with converging radial flow. First, because the inertial effects contribute positively to the magnitude of wall shear stress, with converging flow the range of shear stresses that can be generated for a particular range of radial positions is larger than that for diverging flow under identical conditions. Second, good agreement between the numerical prediction and the inertially corrected solution for creeping flow extends to smaller radial positions with converging flow rather than with diverging flow. This close agreement is shown more clearly by a plot of the departure of the analytical solution for inertially corrected creeping flow from shear stresses predicted with the numerical model for the three volumetric flow rates (Figure 6).

Estimation of minimum radial position and maximum shear stress

To identify the range for which the solutions for creeping flow and creeping flow with an inertial correction are accurate we have selected a maximum departure of 5% of the analytical solution from the corresponding numerical prediction. This criterion results in a minimum radial position that depends on not only the particular model but also the direction of flow and magnitude of volumetric flow rate. For creeping flow at 1.43, 2.15, and 2.86 mL/s this criterion corresponds to radial positions for converging flow of 4.9, 6.1, and, 6.9 mm, respectively, and radial positions for diverging flow of 5.6, 6.8, and 8.4 mm, respectively. These values are comparable to the minimum radial positions for creeping flow predicted by Eq. 9a: 5.3, 6.5, and 7.6 mm for volumetric flow rates of 1.43, 2.15, and 2.86, respectively.

For inertially corrected creeping flow, the departure from the numerical prediction also depends strongly on the direction of flow (Figure 6). For both diverging and converging flow the 5% departure increases radially with increasing volumetric flow rate, but for all three flow rates the distance from the edge of the inlet ($r = 1$ mm) to the minimum radial position for converging flow is half of that distance for diverging flow. Consequently, for the same magnitude of volumetric flow rate, the maximum shear stress—defined here as the inertially corrected solution for creeping flow at the minimum radial position—for converging flow is more than twice that for diverging flow. Values for these minimum radial positions and maximum shear stresses are listed in Table 1.

Analysis of inlet effects associated with converging flow

Reversing the direction of flow has an enormous effect on

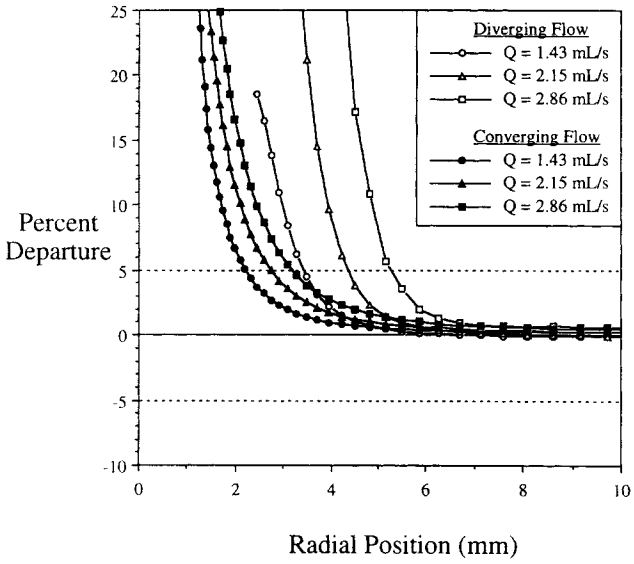

Figure 6. Department of the inertially corrected solution for creeping flow from the numerical calculations.

Horizontal dashed lines at ±5% reflect the criterion for accuracy of the analytical solution. Minimum radial positions —corresponding to departures of 5%—are listed in Table 1.

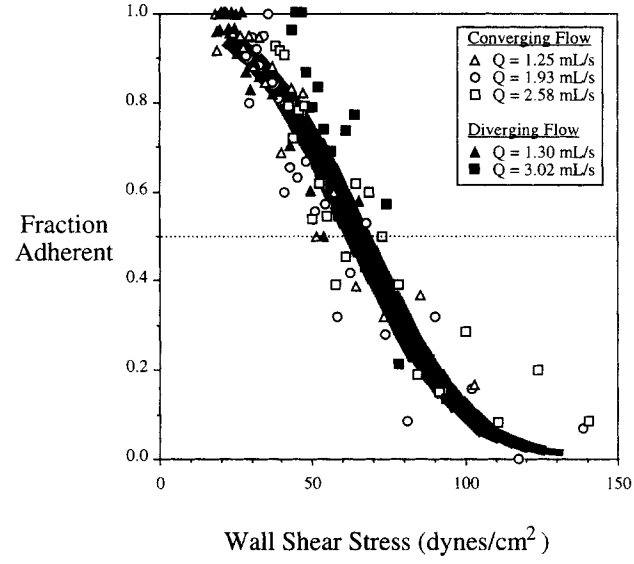

Figure 7. Shear-dependent patterns of adhesion.

Plots of the fraction of murine fibroblasts resisting detachment from fibronectin-coated SAMs of dodecanethiolate as a function of wall shear stress. The shaded region is described by an integral of a normal distribution function (Eq. 10) with parameters, $\tau_{wc} = 64.9 \pm 4.7$ dyne/cm^2 and $\sigma_{\tau_w} = 27.6 \pm 3.9$ dyne/cm^2.

the numerical predictions of shear stresses at small radial positions because laminar flow around a blunt corner requires a recirculation zone downstream. With diverging flow this recirculation zone is outside the inlet and we observe that it propagates to larger radial positions with increasing volumetric flow rate. With converging flow the recirculation zone is in the axially oriented outlet tube. However, with a real radial-flow chamber, entrance/exit effects also should exist at the maximum radial position. In our experimental chamber a corner exists 16 mm from the centerline, and one might expect it to have an effect on shear stresses in this region. To estimate the maximum effect of this corner we numerically modeled this region for converging flow with a volumetric flow rate of 2.86 mL/s (the maximum examined in this study). We found the existence of a small recirculation zone and inlet effects qualitatively similar to those observed for diverging flow at small radial positions. However, because the velocities are significantly smaller here numerical modeling predicts a departure of less than 1% from the solution for creeping flow with an inertial correction at a radial position of 15.5 mm. Therefore, we feel justified in reporting measurements for radial positions within 15 mm—the outer observable region of our chamber—for both converging and diverging flow for volumetric flow rates of at least 2.86 mL/s.

Strength of cell adhesion does not depend on direction or magnitude of flow

Experiments were conducted to measure the strength of adhesion of murine fibroblasts for a range of magnitudes of volumetric flow rate with both converging and diverging flow. Shear-dependent patterns of adhesion were constructed by plotting the fraction of cells that resisted detachment at discrete radial positions against the corresponding shear stress for each position using the inertially corrected solution for creeping flow. These patterns superimposed to a single curve that was independent of the magnitude of volumetric flow rate and direction of flow (Figure 7). Note that no data points were plotted above 100 dyne/cm^2 for diverging flow; only those data for which the shear stress could be estimated reliably were included.

For each individual condition the mean and heterogeneity in the strength of adhesion were determined using Eq. 10

Table 1. Limit for Predicting Shear Stresses*

		Outward Flow		Inward Flow	
Reynolds Number	Volumetric Flow Rate mL/s	Min. Radial Position mm	Max. Shear Stress dyne/cm^2	Min. Radial Position mm	Max. Shear Stress dyne/cm^2
1,000	1.43	3.5	76	2.2	175
1,500	2.15	4.5	90	2.7	220
2,000	2.86	5.3	100	3.3	230

*Minimum radial positions that can be examined quantitatively and local Reynolds number, Re, and shear stress for that position as a function of reference Reynolds number, Re_h, for converging and diverging radial-flow. Minimum radial positions correspond to a maximum departure of 5% of the inertially corrected solution from the numerical predictions. Listed values for shear stress are predicted using the inertially corrected solution (Eq. 6).

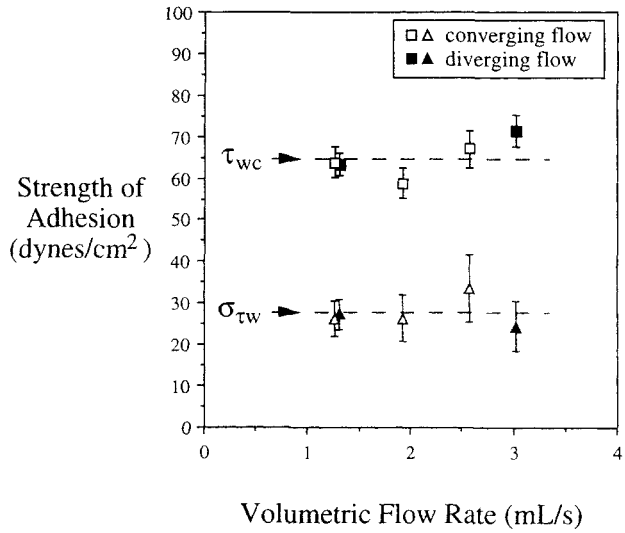

Figure 8. Measured strength of adhesion.

Mean and heterogeneity in the strength of adhesion as a function of volumetric flow rate for converging and diverging flow. Values reflect the best fit of the integral of a normal distribution function (Eq. 10) to data from individual experiments, with error bars corresponding to a marginal confidence interval of 90%.

(Figure 8). The mean strength of adhesion was independent of both volumetric flow rate and direction of flow and had an average value of 64.9 dyne/cm^2 and a standard deviation of 4.7 dyne/cm^2 (7.2% of the mean). This degree of reproducibility is similar to that which we observed previously for diverging flow (Goldstein and DiMilla, 1997). Note that if the strength of adhesion was greater than 100 dyne/cm^2, then its measurement would not be possible for experiments performed with diverging flow. However, for this set of experiments the strength of adhesion was small enough that measurements for diverging and converging flow could be compared and large enough that the inertial correction is important: for converging flow the inertial term increased the mean strength of adhesion by 3 to 6% and for diverging flow it reduced measurements by 4 to 8%. Not including the inertial correction resulted in poorer correspondence between data for converging and diverging flow. The heterogeneity in the strength of adhesion also was independent of experimental conditions and had an average value of 27.6 dyne/cm^2 and a standard deviation of 3.9 dyne/cm^2. Finally, the average values for mean and heterogeneity in the strength of adhesion were plotted (the shaded region in Figure 7) to demonstrate that the shear-dependent patterns of adhesion are described well by Eq. 10.

Experiments with converging flow also demonstrated the recirculation zone near the lower surface at $r < 1$ mm that was predicted numerically (Figure 9). The two separate clusters of cells indicated the presence of two stagnation zones: an inner one at the axis of symmetry (center of Figure 9a) and an outer one where the direction of shear reverses (Figure 9b and the edges in Figure 9a). In addition, cells near the axis of symmetry had a tear-drop shape that indicated they were elongated radially outward by recirculating flow.

Finally, several practical advantages also exist for operating the radial-flow chamber with converging flow. With diverging flow, cells that are detached at high shear stresses move in the direction of decreasing shear stress and may either interfere with adherent cells at lower shear stresses or reattach to the substrata. In addition, because cell suspensions are introduced into the closed chamber by the axial tube at the center line, many nonadherent cells can remain in this line until flow is applied. With converging flow these detached or nonadherent cells are less likely to disturb adherent cells. Another advantage we discovered with converging flow is that air bubbles—which can have a detrimental effect on the quality of experimental results (Goldstein and DiMilla, 1997; Cozens-Roberts et al., 1990)—remain trapped in the larger outer reservoir of the radial-flow chamber.

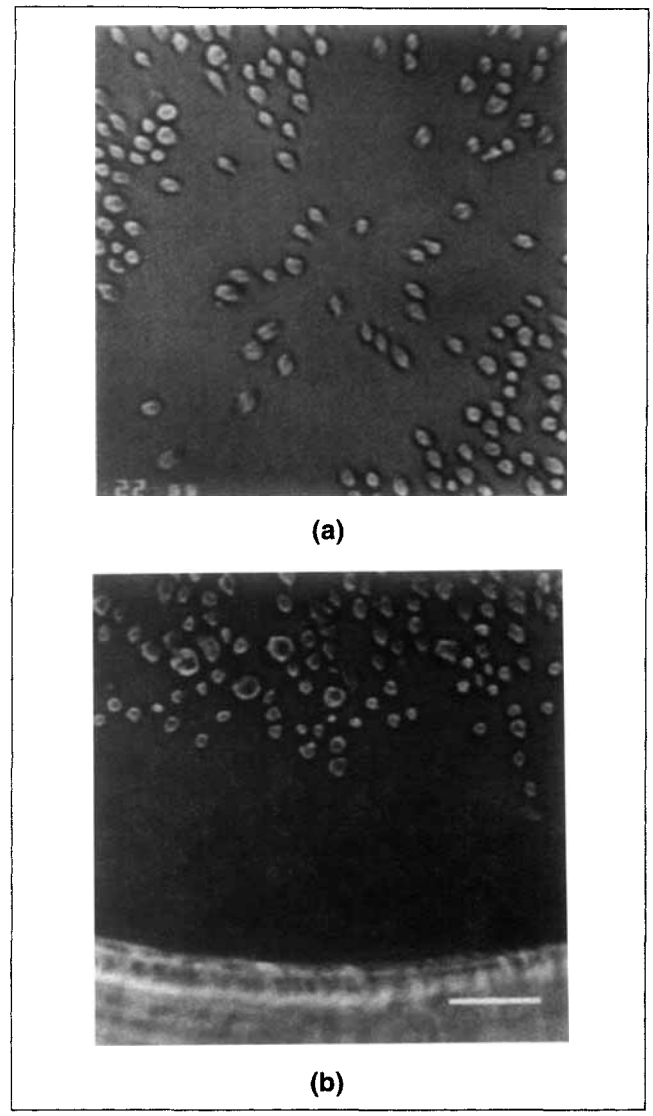

Figure 9. Images of cell resisting detachment.

(a) At the centerline, revealing two stagnation regions. (b) At the edge of inlet, showing the outer portion of the outer stagnation region. Volumetric flow rate was 2.58 mL/s. The scale bar corresponds to 100 μm.

Conclusions

In this study the advantages of operating an RFC with converging flow were demonstrated using a numerical and two

analytical models for radial flow. The fluid mechanics at small radial positions—where corner and inertial effects limit the maximum shear stresses that can be predicted accurately—were examined for converging and diverging flow. With diverging flow the corner produces a recirculation zone that extends to increasing radial positions with increasing volumetric flow rate and limits the minimum radial position for which quantitative predictions are reliable. With converging flow this recirculation zone is confined to the axially-oriented tube and permits accurate prediction of shear stress at smaller radial positions. In addition, inertial effects differ with the direction of flow: they increase the magnitude of the wall shear stress for converging flow but decrease the magnitude for diverging flow. Analytical solutions for creeping flow and creeping flow with an inertial correction were compared with numerical predictions to determine the minimum radial positions and the maximum wall shear stresses for which these analytical solutions are valid. For the solution for creeping flow with an inertial correction the maximum wall shear stress for converging flow is more than twice as large as that for diverging flow. Experimental studies were performed to demonstrate that the strength of cell adhesion to model surfaces—using the solution for creeping flow with an inertial correction—was independent of the direction of flow and volumetric flow rate. This study provides guidelines for operation and quantitative prediction of wall shear stresses necessary to examine cell interactions with biomaterials in RFCs.

Acknowledgments

The authors thank Dennis Prieve for suggestions on the mathematics, Stephen Garoff for use of a thermal evaporator to prepare test surfaces, Charlotte Bartosh for help with cell culture, and João Albuquerque for computer programming of an algorithm for fitting nonlinear data.

This work was supported by NSF Grant BES-9410215 and a Searle Scholars Award to P. A. D., a graduate fellowship through the NSF Graduate Research Traineeship Program Grant BIR-9256343 to A. S. G., and indirectly through NSF Grant MCB-8920118 to the Center for Light Microscope Imaging and Biotechnology.

Literature Cited

Chu, L., L. A. Tempelman, C. Miller, and D. A. Hammer, "Centrifugation Assay of IgE-Mediated Rat Basophilic Leukemia Cell Adhesion to Antigen-Coated Polyacrylimide Gels," *AIChE J.*, **40**, 692 (1994).

Cozens-Roberts, C., J. A. Quinn, and D.A. Lauffenburger, "Receptor-Mediated Adhesion Phenomena: Model Studies with the Radial-Flow Detachment Assay," *Biophys. J.*, **58**, 107 (1990).

Dickinson, R. B., and S. L. Cooper, "Analysis of Shear-Dependent Bacterial Adhesion Kinetics to Biomaterial Surfaces," *AIChE J.*, **41**, 2160 (1995).

DiMilla, P. A., J. P. Folkers, H. A. Biebuyck, R. Härter, G. P. López, and G. M. Whitesides, "Wetting and Protein Adsorption on Self-Assembled Monolayers of Alkanethiolates Supported on Transparent Films of Gold," *J. Amer. Chem. Soc.*, **116**, 2225 (1994).

Evans, E., D. Berk, and A. Leung, "Detachment of Agglutinin-Bonded Red Blood Cells: I. Forces to Rupture Molecular-Point Attachments," *Biophys. J.*, **59**, 838 (1991).

Finger, E. B., K. D. Puri, R. Alon, M. B. Lawrence, U. H. von Andrian, and T. A. Springer, "Adhesion Through L-Selectin Requires a Threshold Hydrodynamic Shear," *Nature*, **379**, 266 (1996).

Fowler, H. W., and A. J. McKay, "The Measurement of Microbial Adhesion," *Microbial Adhesion to Surfaces*, R. C. W. Berkeley, J. M. Lynch, J. Melling, P. R. Rutter, and B. Vincent, eds., Ellis Horwood, Chichester, England, p. 143 (1980).

Fryer, P. J., K. H. Slater, and J.E. Duddridge, "Suggestions for the Operation of Radial Flow Cells in Cell Adhesion and Biofouling Studies," *Biotechnol. Bioeng.*, **27**, 434 (1985).

Goldstein, A. S., and P. A. DiMilla, "Application of Fluid Mechanic and Kinetic Models to Characterize Mammalian Cell Detachment in a Radial-Flow Chamber," *Biotechnol. Bioeng.*, **55**, 616 (1997).

Hammer, D. A., and D. A. Lauffenburger, "A Dynamic Model for Receptor-Mediated Cell Adhesion to Surfaces," *Biophys. J.*, **52**, 475 (1987).

Hunt, J. B., and I. Torbe, "Characteristics of a Hydrostatic Thrust Bearing," *Int. J. Mech. Sci.*, **4**, 503 (1962).

Jackson, J. D., and G. R. Symmons, "The Pressure Distribution in a Hydrostatic Thrust Bearing," *Int. J. Mech. Sci.*, **7**, 239 (1965).

Jackson, J. D., and G. R. Symmons, "An Investigation of Laminar Radial Flow Between Two Parallel Discs," *Appl. Sci. Res. A.*, **15**, 59 (1966).

Kuo, S. C., and D. A. Lauffenburger, "Relationship Between Receptor/Ligand Affinity and Adhesion Strength," *Biophys. J.*, **65**, 2191 (1993).

McIntire, L. V., R. Alevriadou, J. L. Moake, and Z. M. Ruggeri, "Platelet Surface Glycoprotein IB Binding Site of von Willebrand Factor Mediates Platelet Adhesion to Collagen under Flow Conditions," *Ann. Biomed. Eng.*, **19**, 606 (1991).

Moller, P. S., "Radial Flow Without Swirl Between Parallel Discs," *Aeronaut. Q.*, **14**, 163 (1963).

Rezania, A., C. H. Thomas, and K. E. Healy, "A Probabilistic Approach to Measure the Strength of Bone Cell Adhesion to Chemically Modified Surfaces," *Ann. Biomed. Eng.*, **25**, 190 (1997).

Sadahiro, M., T. O. McDonald, and M. D. Allen, "Reduction in Cellular and Vascular Rejection by Blocking Leukocyte Adhesion Molecule Receptors," *Amer. J. Pathol.*, **142**, 675 (1993).

Truskey, G. A., and J. S. Pirone, "The Effect of Fluid Shear Upon Cell Adhesion to Fibronectin-Treated Surfaces," *J. Biomed. Mat. Res.*, **24**, 1333 (1990).

Usami, S., H.-H. Chen, Y. Zhao, S. Chien, and R. Skalak, "Design and Construction of a Linear Shear Stress Flow Chamber," *Ann. Biomed. Eng.*, **21**, 77 (1993).

van Kooten, T. G., J. M. Schakenraad, H. C. van der Mei, and H. J. Busscher, "Development and Use of a Parallel-Plate Flow Chamber for Studying Cellular Adhesion to Solid Surfaces," *J. Biomed. Mat. Res.*, **26**, 725 (1992).

Williams, S. K., D. G. Rose, and B. E. Jarrell, "Microvascular Endothelial Cell Sodding of ePTFE Vascular Grafts: Improved Patency and Stability of the Cellular Lining," *J. Biomed. Mat. Res.*, **28**, 203 (1994).

Xiao, Y., and G. A. Truskey, "Effect of Receptor-Ligand Affinity on the Strength of Endothelial Cell Adhesion," *Biophys. J.*, **71**, 2869 (1996).

Manuscript received May 16, 1997, and revision received Sept. 18, 1997.